Key Engineering Materials
ISSN: 1662-9795, Vol. 926, pp 176-186
doi:10.4028/p-6p7o75

Submitted: 2021-12-08
Accepted: 2022-02-18
Online: 2022-07-22

Efficient Build-Up of High-Strength Aluminum Structures Using Friction Stir Additive Manufacturing

Martina E. Sigl[1,a*], Paula Danninger[1,b], Christian Bernauer[1,c], Roman Hartl[1,d], and Michael F. Zaeh[1,e]

[1*]Institute for Machine Tools and Industrial Management (*iwb*),
TUM School of Engineering and Design,
Technical University of Munich, Boltzmannstr. 15, 85748 Garching, Germany

[a]Martina.Sigl@iwb.tum.de, [b]Paula.Danninger@tum.de, [c]Christian.Bernauer@iwb.tum.de,
[d]Roman.Hartl@iwb.tum.de, [e]Michael.Zaeh@iwb.tum.de

Keywords: Friction stir additive manufacturing; friction stir lap welding; friction stir welding; temperature control; EN AW-7075; stationary shoulder

Abstract. Friction Stir Additive Manufacturing (FSAM) is a novel process with which large-scale aluminum structures can be produced from high-strength alloys such as the 7xxx series. Due to the prevalence of these alloys in airplanes and rockets, the process offers high application potential, for example in fabricating stringers and stiffeners. The building process in FSAM is characterized by sequentially stacking and friction stir lap welding (FSLW) metal sheets. Before adding the next layer, the surface is machined (i.e., by milling). So far, this is a necessary step to enable gap-free welding of the layers, which results in increased costs and reduced layer heights. The investigations described in this paper were aimed at improving the weld surface quality to enable defect-free FSAM without the additional machining step. For this, FSLW was conducted using different welding tools. The resulting welds were evaluated based on superficial and internal characteristics as well as the mechanical properties (shear strength). With a welding tool in which both a rotating and a stationary shoulder were combined, defect-free weld seams with a mean underfill and a mean flash height of 0.07 mm were produced. In a subsequent study, it was proven that defect-free FSAM without surface machining is possible up to the fifth layer using the combined welding tool.

Introduction

Friction Stir Additive Manufacturing (FSAM) is an innovative additive manufacturing process in which metal sheets (e.g., aluminum [1] or magnesium [2]) are subsequently stacked on a platform and joined by friction stir lap welding (FSLW). Thereby, a rotating tool, consisting of a probe and a shoulder, is plunged into the stacked sheets. Frictional heat is generated, which causes the material in the process zone around the tool to be softened. In combination with the rotary movement (*tool rotational speed n*), a material flow is generated and the stacked sheets are joined. After plunging, the tool remains in the dwell phase to increase the energy input into the weld. Subsequently, the tool is moved along a welding trajectory at a *welding speed v*, while it is pressed against the workpiece with an *axial force* F_z. The weld produced is asymmetric: on the *advancing side* (AS), the tool's direction of rotation coincides with the direction of the welding trajectory. The other side of the weld is called the *retreating side* (RS). At the end of the trajectory, the tool is retracted, leaving a negative of the probe and the shoulder on the surface of the workpiece (exit hole). In preparation for building the next layer and to ensure a gap-free welding process, the surface is machined [2].

Only a few studies have investigated the new FSAM process. Table 1 shows a summary of the build heights achieved using FSAM. Considering the height of the final additive build h_a, the sheet thicknesses $h_{sheet,\,i}$ for each layer i as well as the total number of layers n, the *material utilization ratio* with regards to the heights $p_{mur,\,h}$ is calculated by

$$p_{mur,\,h} = h_a / \left(\sum_{i=1}^{n} i \cdot h_{sheet,\,i} \right). \quad (1)$$

The highest $p_{mur,\,h}$ (93.3%) was achieved by Yuqing et al. [3], who produced a nine-layer build (platform included) of AA7075-O, while the lowest $p_{mur,\,h}$ (79.4%) was obtained by Palanivel et al. [1] who built four layers (platform included) of the magnesium alloy Mg-4Y-3Nd-T5.

The amount of material, which has to be removed through machining, depends on the weld topography. The surface properties result from the material softening and flow beneath the shoulder. Factors influencing these are the process parameters (e.g., the tool's *tilt angle* α [4]) as well as the geometry (e.g., the diameter d_s [4] and the shape [5]) of the shoulder area that is in contact with the workpiece [5]. Values taken from the literature are listed in Table 1. Aside from conventional tools, *stationary shoulder* tools can be used to further improve the surface of friction stir lap welds [6].

Table 1: Analysis of the build heights h_a and material utilization ratios $p_{mur,\,h}$ taken from literature data; missing data is marked with "–"

Material with temper state	Sheet thickness $h_{sheet,\,i}$ in mm	Number of layers n —	Tilt angle α in °	Shoulder geometry —	Shoulder diameter d_s in mm	Total build height h_a [1] in mm	Material utilization ratio $p_{mur,\,h}$ [2] in %	Reference
Mg-4Y-3Nd-T5	1.7	4 [1]	1.5°	concave	11.8	5.4	79.4	Palanivel et al. [1]
AA5083-O	3.17	4 [1]	1.5°	concave	10.0	11.2	88.3	Palanivel et al. [1]
2195-T8 [3]	2	5 [1]	—	concave [4]	18.0	9.25 [5]	92.5	Zhao et al. [7]
AA6061-T6	4	2	—	—	24.0	—	—	Zhang et al. [8]
AA7075-O	5	9 [1]	2°	concave	30.0	42.0	93.3	Yuqing et al. [3]

[1] Platform included
[2] Calculated by using Eq. 1
[3] No standard given
[4] Identified by the authors of the present publication from a photograph of the tools
[5] Measured by the authors of the present publication from a photograph of a cross section and compensating the platform thickness

The state of the art can be summarized as follows:

- In FSAM, the surface of each welded sheet is machined in order to ensure zero gap for the subsequent welding process. This reduces the layer height and efficiency of the process.
- Factors influencing the weld surface are the process parameters and the geometry of the FSW tool. With stationary shoulder tools, smooth surfaces can be produced for FSLW [6].
- Previous investigations for FSAM [1, 3, 7] were performed using conventional FSW tools with a concave featureless shoulder. The shoulder diameters d_s ranged from 10 mm to 30 mm and the tilt angles α from 1.5° to 2° (Table 1).

Methodology

Objective. The objective of the investigations was to achieve improved weld surfaces in FSAM, which reduces the effort for the machining process step before building the next layer. This leads to a more efficient process and an increased material utilization rate regarding the build heights $p_{mur,\,h}$.

Research Approach. Three experimental studies were conducted with different FSW tools. In preceding screening experiments, different shoulder geometries (concave and flat) and features (with/without scrolls) were investigated to identify a suitable tool and parameter window. Then, using the identified tool, two parameter studies were conducted in which the welding temperature T_p, the welding speed v, and the axial force F_z were varied (studies 1 and 2). A second parameter study (study 2) was conducted in which the tool from study 1 was combined with a stationary shoulder. In a subsequent study (study 3), a five-layer FSAM build was produced using three different parameter sets and without the machining process step.

All weld surfaces produced were inspected visually and by topographical as well as metallographic analysis. In addition, shear testing was performed in studies 1 and 2 to determine cause-effect-relationships between the weld quality and the mechanical properties. The experimental setup and methods that were used are described below.

Experimental Setup. The welding experiments were conducted using an industrial robot (KR 500-2 MT, KUKA AG, Augsburg, Germany), which was equipped with an FSW spindle (RS XXXX000-0784, CyTec Zylindertechnik GmbH, Jülich, Germany). The axial force F_z was measured by load cells above the spindle and was internally controlled. Sheathed thermocouples (type K, 443-7967, RS Components GmbH, Frankfurt am Main, Germany) with a diameter of 0.5 mm were glued (COT Resbond 989-1, Polytec PT GmbH, Karlsbad, Germany) into the FSW tool to acquire the temperatures inside the weld during the process (Fig. 2). A temperature measuring tool [9] was used to process the thermocouple signals. To compensate for the cooling effect of the stationary shoulder [6] and to ensure more similar welding conditions when applying different tools [10], closed-loop temperature control was applied as described by Bachmann et al. [11]. The control algorithm was implemented in a real-time system (MicroLabBox, dSPACE GmbH, Paderborn, Germany). Further information regarding the research machine setup is given in [12].

In the experiments, aluminum sheets (300 mm × 50 mm × 4 mm, Fig. 1) of the high-strength alloy EN AW-7075-T6 were friction stir lap welded. The aluminum sheets were clamped on each short side with the same screw torque (40 Nm). The stacking configuration for studies 1 and 2 was chosen so that lower shear strengths were to be expected. The literature [13] suggests that this is the case when the RS lies on the wide side of the upper sheet (Fig. 1a). The decision was based on the assumption that the overall strength in later FSAM builds (Fig. 1b) is determined by the strength of the weakest side. For study 3, the sheets were stacked so that they fully overlapped (Fig. 1b). To prevent the collision of the tool with the clamping claws, the weld lengths in studies 2 and 3 were reduced. The exit holes in study 3 were filled with epoxy resin (aluminum repair stick, Engelbert Strauss GmbH & Co. KG, Biebergemünd, Germany) in order not to leave them empty for the build-up of the next layer and thus to prevent instabilities in the force controlled process.

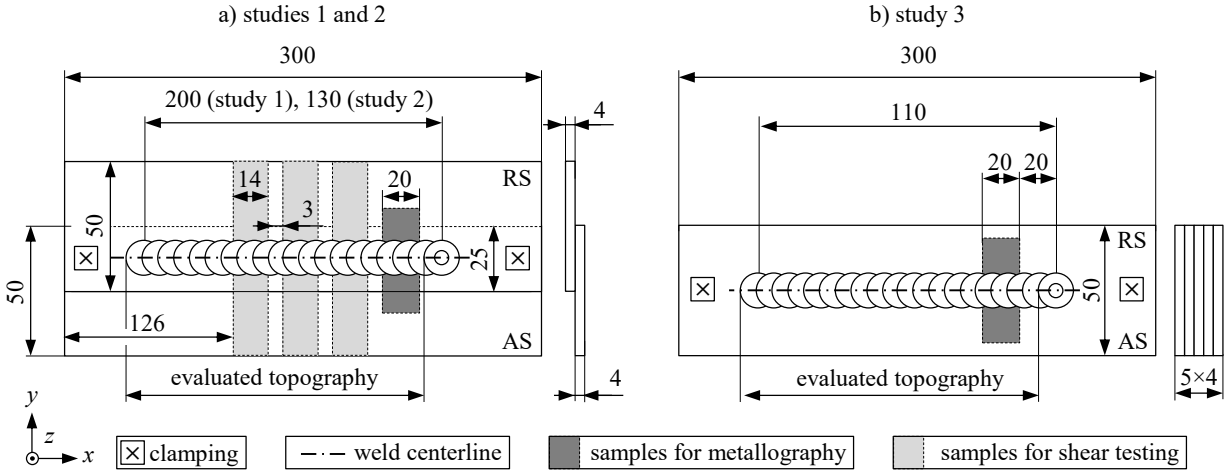

Fig. 1: Sketches of the sample configurations a) for studies 1 and 2 as well as b) for study 3; geometrical values are not to scale and are given in mm

For studies 1 – 3, a standard FSW tool, consisting of a rotating shoulder and a threaded conical probe with three flats, was used. The diameter of the shoulder d_s (16 mm) was determined from the base diameter of the probe d_p (8 mm) in accordance with the design guidelines given by FULLER [14], who suggests a ratio between the shoulder diameter d_s and the probe diameter d_p from 2 to 3. Due to the negative geometric influence of the shoulder diameter on the heel plunge depth, the lowest ratio from this interval (2) was chosen. The shoulder shape (flat and double-scrolled) was selected based on screening experiments. For studies 2 and 3, the tool was combined with an additional stationary shoulder with an outer diameter d_{ss} of 20 mm (Fig. 2).

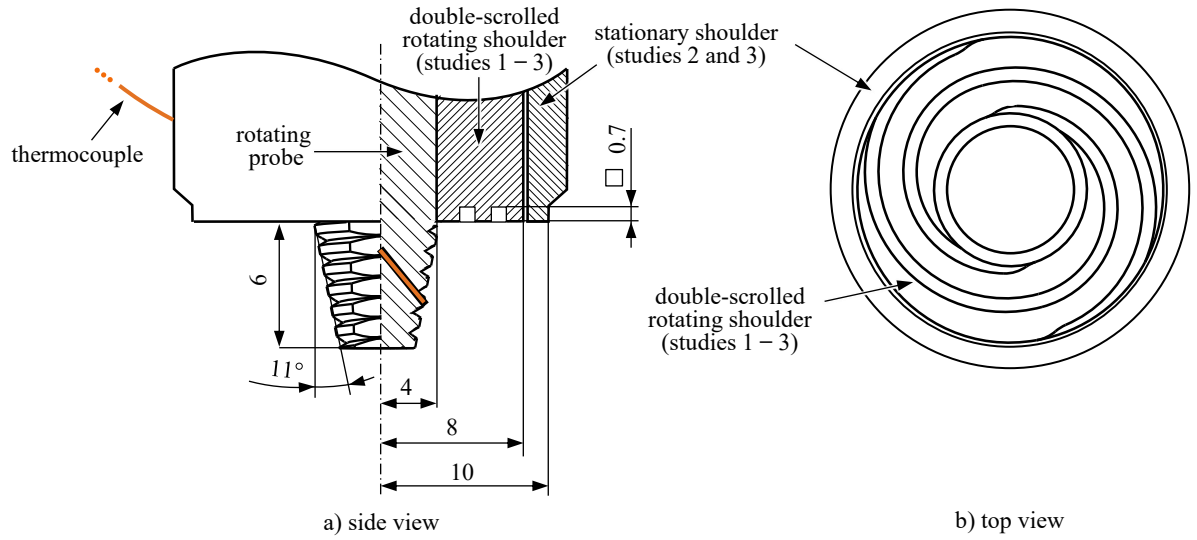

Fig. 2: Sketch of the FSW tools in side (a) and top (b) view: with a rotating shoulder (studies 1 – 3) and in combination with a stationary shoulder (studies 2 and 3); geometrical values are not to scale and are given in mm if not otherwise indicated

A total of 15 welds were produced in each study (45 in total). The experiments in studies 1 and 2 were conducted following a central composite design (CCD), which is a combination of a cube- and a star-shaped experimental plan. This enables the efficient experimental investigation of nonlinear effects. Table 2 shows the process parameters chosen for the conducted experiments. In study 3, the additive builds were produced with three process parameter sets chosen from study 2. Temperature control was activated during the dwell phase of the welding process. The feed motion was started once the set temperature T_p had been reached. The probe length l_p (6 mm), the rotational speed during the plunging of the FSW tool n_0 (2000 r/min), and the tilt angle α (0.5°) were determined during the screening experiments. A low tilt angle value α was chosen because it geometrically influences the plunge depth of the tool heel [4] and therefore the seam underfill. Due to the low stiffness of the welding robot and the higher forces when welding with a stationary shoulder, a higher tilt angle of 1° and a lower welding speed v were necessary in studies 2 and 3 compared to study 1. The larger diameter of the stationary shoulder (20 mm) also resulted in a higher axial force F_z for studies 2 and 3.

Table 2: Welding parameters for studies 1 – 3; the full experimental plan is shown in Table 3 and 4

	Study 1 with a rotating shoulder and a tilt angle α of 0.5°			Study 2 with a rotating and a stationary shoulder as well as a tilt angle α of 1°			Study 3 with a rotating and a stationary shoulder as well as a tilt angle α of 1° (selected parameters from study 2)		
Factor level	Welding temperature T_p in °C	Welding speed v in mm/min	Axial force F_z in kN	Welding temperature T_p in °C	Welding speed v in mm/min	Axial force F_z in kN	Welding temperature T_p in °C	Welding speed v in mm/min	Axial force F_z in kN
--	470	50	6.0	470	35	7.0	–	–	–
-	480	100	6.5	480	50	7.5	–	–	–
0	490	150	7.0	490	65	8.0	490	65	8.0
+	500	200	7.5	500	80	8.5	500	80	8.5
++	510	250	8.0	510	95	9.0	–	95	–

Visual Inspection. All weld seams were visually inspected and categorized into four *classes* (Fig. 3): *a*) “flawless”, *b*) “acceptable with flash”, *c*) “acceptable with minor imperfections” and *d*) “unacceptable” (with major defects like surface lack of fill).

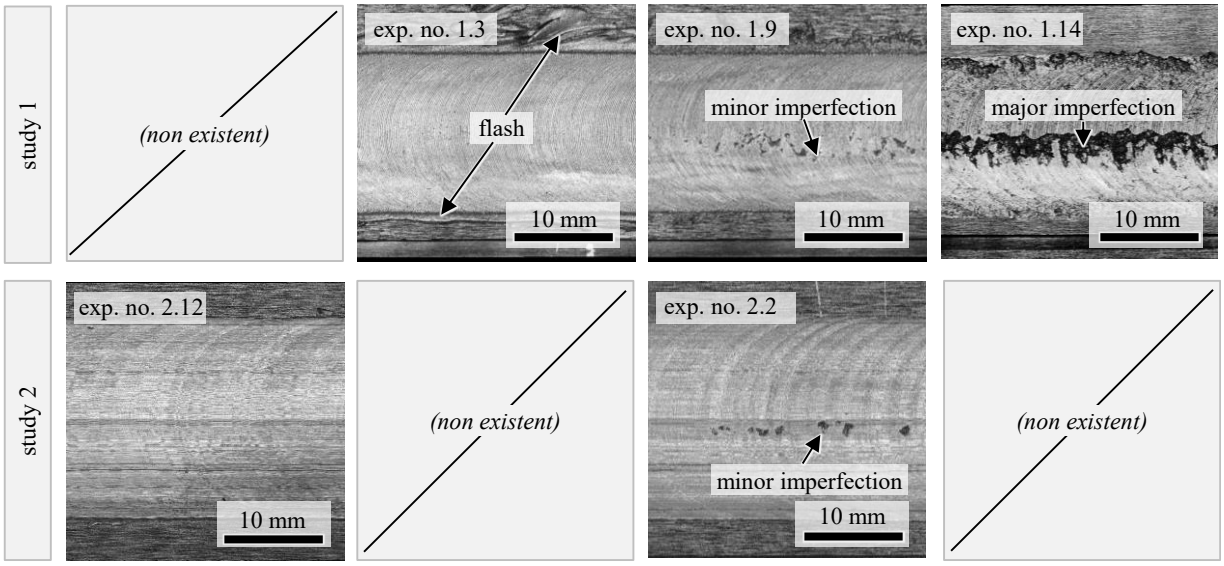

class a: ● flawless weld surface quality

class b: ▲ acceptable weld surface quality with flash

class c: ■ acceptable weld surface quality with minor imperfection

class d: ◆ unacceptable weld surface quality

Fig. 3: Weld examples for the surface quality *classes a – d* from studies 1 and 2. Different markers (e.g., the green circle) are assigned to the classed and are used in Fig. 4

Topography Analysis. All welds from *classes a* and *b* (studies 1 – 3) were scanned using a three-dimensional profilometer (VR-3100, Keyence Corporation, Osaka, Japan). The weld surfaces were captured with a 12-fold magnification and a measurement accuracy of 3 µm in the *z*-direction and 5 µm in the *x*- and *y*-directions. Distortions during welding were removed from the data as described by Hartl et al. [5]. Afterwards, the reference plane was set as the sheet surface surrounding the weld. With the exception of the exit hole area, the whole weld surface was evaluated (Fig. 1). The mean ($\bar{h}_f$ and $\bar{h}_{su}$), the maximum ($\hat{h}_f$ [5] and $\hat{h}_{su}$) and the standard deviation ($h_{f,\,sd}$ [5] and $h_{su,\,sd}$ [5]) values of the flash heights as well as the maximum seam underfills along the weld centerline were used as indicators for evaluating the weld seam quality.

Metallographic Analysis. A cross-section sample was taken from each weld (studies 1 and 2) and each additive build (study 3) as shown in Fig. 1 using a wet cut-off grinder. The samples from studies 1 and 2 were embedded in epoxy resin for stabilization. All samples were ground, polished with 1 µm cotton cloth, and micro-etched with Kroll's reagent. The cross-section characteristics were recorded using a microscope (MM-40, Nikon, Tokyo, Japan) and the above-mentioned profilometer.

Shear Testing. Three shear specimens were taken from each weld of studies 1 and 2 (Fig. 1a) with a surface quality within *classes a – c*. In contrast to the topographical investigations, welds from *class c* were also taken into consideration because it was assumed that minor imperfections do not significantly influence the shear strength. The specimens were milled to a width of 14 mm. A material testing machine (Z050, AllroundLine, ZwickRoell GmbH & Co. KG, Ulm, Germany) was used to determine the shear force F_n. The shear tests were performed at room temperature at an initial strain rate of 0.23×10^{-3} 1/s. The mean ($\bar{F}_n$), the maximum ($\hat{F}_n$) and the standard deviation ($F_{n,\,sd}$) values of the three measurements were determined for each weld.

Results and Discussion

A summary of all collected data is given in Table 3 and 4 (see Appendix). The first digit of the experiment number (exp. no.) corresponds to the study, the second to the part and the last digit in study 3 to the layer number. In the following, the data resulting from the conducted experiments are elaborated on and discussed.

Weld Surfaces in Studies 1 and 2. In Fig. 4, the achieved surface qualities for each conducted experiment of studies 1 (Fig. 4a) and 2 (Fig. 4b) are displayed. The horizontal axis is used for depicting the welding temperature levels T_p. The two vertical axes show the levels of the welding speed v (left) and of the axial force F_z (right). Each of the 15 data points corresponds to one conducted experi-ment. The shape and color of the data points are assigned to the surface quality *classes a – d* (Fig. 3). An example (exp. no. 1.3) with the corresponding welding parameters is shown in Fig. 4a.

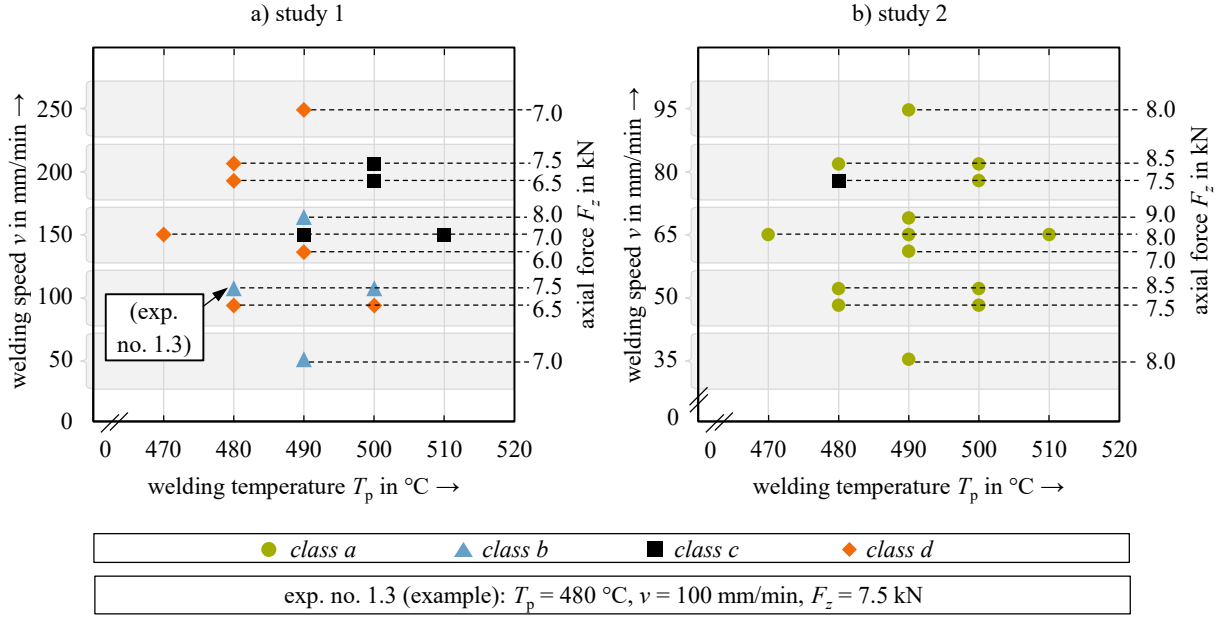

Fig. 4: Weld surface qualities for the process parameters welding temperature T_p, welding speed v, and axial force F_z (Table 3) of studies 1 (a) and 2 (b); examples of the surface quality classes are depicted in Fig. 3

In study 1 (Fig. 4a), only four out of the 15 welds presented a completely filled surface, which was accompanied by flash (*class b*). These welds were produced by applying low to medium welding speeds v, combined with medium to high axial forces F_z. The welding experiment with the lowest welding speed v (50 mm/min, exp. no. 1.10) had to be stopped prematurely because of an increasing plunging of the tool. Unacceptable weld surface qualities (*class d*) resulted when applying low to medium axial forces F_z and/or low to medium welding temperatures T_p. Weld surfaces with minor imperfections (*class c*) were produced by using higher welding temperatures T_p in combination with medium axial forces F_z. No welds with a surface quality *class a* could be produced in study 1. A topographical analysis was therefore only conducted for welds of *class b*. The maximum seam underfill $\hat{h}_{su}$ (0.85 mm) and the maximum flash height $\hat{h}_f$ (4.32 mm) were lowest in exp. no. 1.13 and 1.3 respectively.

In contrast, with the stationary shoulder tool in study 2 (Fig. 4b), almost all welds were classified as “flawless” with respect to their surface quality (*class a*). The seam underfills $\hat{h}_{su}$ ranged from maximum values of 0.36 mm (exp. no. 2.6) to 0.55 mm (exp. no. 2.5). Only one of the weld surfaces (exp. no. 2.2, *class c*) displayed minor imperfections. This was welded with a parameter set in which a higher welding speed v (80 mm/min), a lower welding temperature T_p (480 °C), and a lower axial force F_z (7.5 kN) were combined, which could have resulted in an insufficient compression of the weld and therefore caused the imperfection.

Weld Morphologies in Studies 1 and 2. Only one parameter set in study 1 (exp. no. 1.7) produced welds without cavities inside the weld nugget, in contrast to five (exp. no. 2.3, 2.6, and 2.8 – 2.10) of the 15 welds of study 2. Hooking was visible in all cross sections (example in Fig. 5). The welds of study 2 without cavities all exhibited a greater flash height (maximum values $\hat{h}_f$ above 0.68 mm and mean values $\bar{h}_f$ above 0.15 mm). It can therefore be assumed that the appearance of cavities is negatively correlated to the flash height.

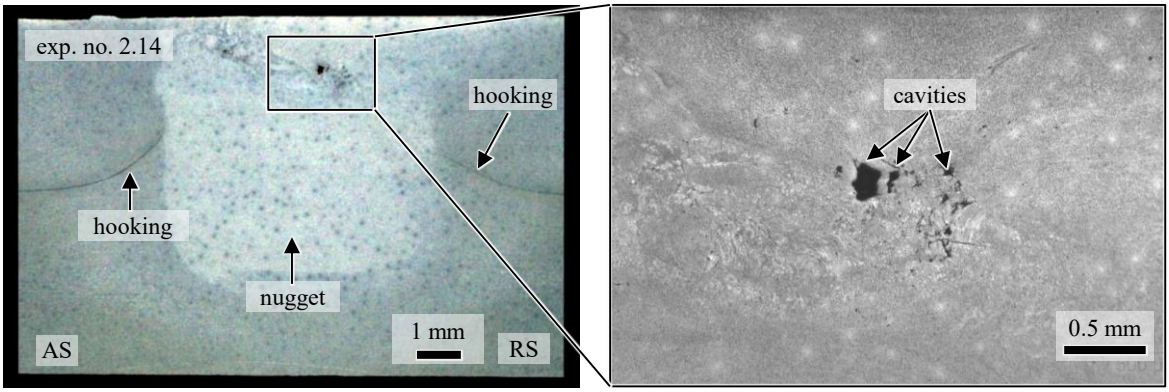

Fig. 5: Example of a weld cross section (exp. no. 2.14) showing cavities inside the nugget and hooking

Shear Forces in Studies 1 and 2. Shear forces F_n were measured for all welds without major imperfections (*classes a – c*). The mean values ($\overline{F}_n$) ranged from 6.31 kN (exp. no. 2.7) to 10.70 kN (exp. no. 2.2) and the standard deviations within each weld from 0.05 kN (exp. no. 1.18) to 0.51 kN (exp. no. 2.2). No correlation to the weld topography was detected. Welds that could withstand higher shear forces $\overline{F}_n$ above 9.5 kN were found for both studies and in each of the tested surface quality *classes a – c*. These welds all displayed internal cavities. The six welds without cavities (exp. no. 1.7, 2.3, 2.6, 2.8 – 2.10) exhibited reduced strengths with mean shear forces $\overline{F}_n$ lower than 8.33 kN. From this analysis, it can be assumed that cavities or minor superficial imperfections do not reduce the overall shear strength of the welds. The fracture pattern (Fig. 6) suggests that the cause for reduced strengths was instead hooking, which facilitated crack initiation. The literature [15, 16] supports this hypothesis, as shear strengths increased with rising welding speeds v (Table 3), which results in lower hooking heights [15].

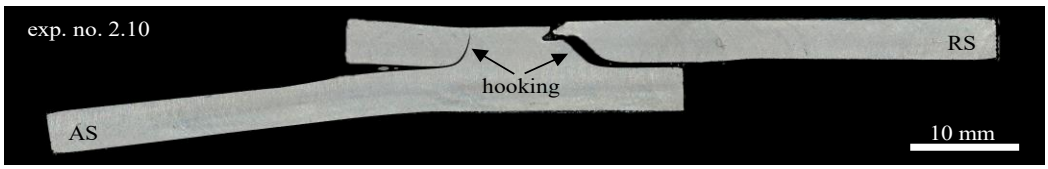

Fig. 6: Fracture pattern of one shear test sample of exp. no. 2.10 (without cavities)

Weld Surfaces and Morphologies in Study 3. Finally, FSAM was performed using the combined tool from study 2 and without the machining process step. Three different parameter sets were chosen: The parameter set that produced the lowest mean seam underfill and flash (exp. no. 2.11 for 3.3) as well as two parameter sets that did not result in any cavities in study 2 (exp. no. 2.8 and 2.9 for 3.1 and 3.2).

Fig. 7 shows that the mean seam underfills $\overline{h}_{su}$ steadily increased with every layer in an almost linear relation for all parameter sets. The weld surface qualities declined in the higher layers of the additive build (Table 4). The best result with regards to the surface and the internal quality was obtained with a high welding temperature T_p of 500 °C and axial force F_z of 8.5 kN (exp. no. 3.1, Fig. 8). With that, the weld surface quality declined as late as in the final layer (exp. no. 3.1.5) from *class a* (Fig. 8c) to *c* (Fig. 8b). Within almost every layer (except exp. no. 5.1.2 and 5.1.3) the lowest maximum seam underfill values $\hat{h}_{su}$ (0.47 mm – 0.74 mm) and flash heights $\hat{h}_f$ (0.47 mm – 0.60 mm) were achieved with this process parameter set. The lowest mean seam underfills $\overline{h}_{su}$ (0.03 mm – 0.19 mm) and flash heights $\overline{h}_f$ (0.07 mm – 0.14 mm), however, resulted from a parameter set (exp. no. 3.3) in which a lower welding temperature (490 °C), the highest welding speed (95 mm/min), and a lower axial force F_z (8.0 kN) were combined.

It is therefore assumed that seam underfills can be compensated up to a certain point by welding with higher temperatures T_p and axial forces F_z, as this results in an increased deformation of the material. With slightly lower welding temperatures T_p and axial forces F_z, cavities formed (exp. no. 3.2.4) or the surface quality started to degrade as early as in the fourth layer (exp. no. 3.2.4 and 3.1.4).

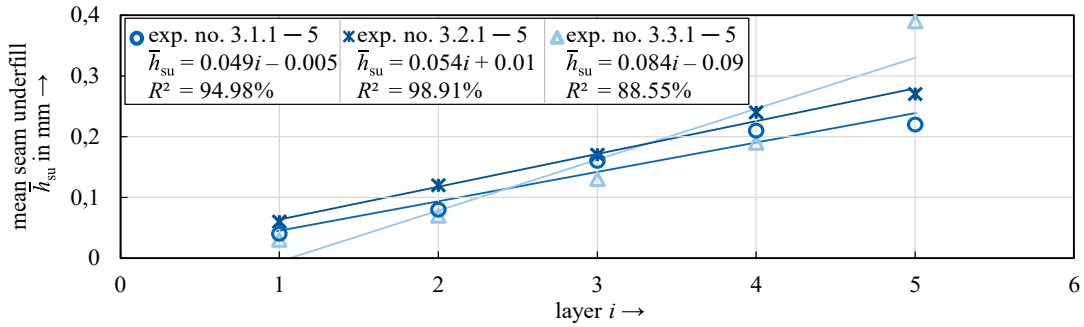

Fig. 7: Mean values of the seam underfills $\bar{h}_{su}$ for each weld of the five layers i in study 3

In contrast to the friction stir lap welds, which were produced with the same process parameters in study 2 (exp. no. 2.11), no cavities were visible in the first three layers of the additive build (exp. no. 3.3.1 – 3.3.3). Several reasons for this discrepancy are possible: Cavities could have been irregularly distributed along the weld, which means it cannot be guaranteed that all cavities are detectable in cross sections. Another possibility is that smaller cavities on the upper part of the seam are broken up when restirring the material during the welding of the next layer.

Formation of weld defects in higher layers was also observed by Zhao et al. [7] and Palanivel et al. [2], which they attributed to different thermal conditions in the layers. Because of the use of temperature control in study 3, it is hypothesized that the defects in the higher layers of this study are, however, the result of insufficient compression during welding caused by the increased gap between the metal sheets (Fig. 7).

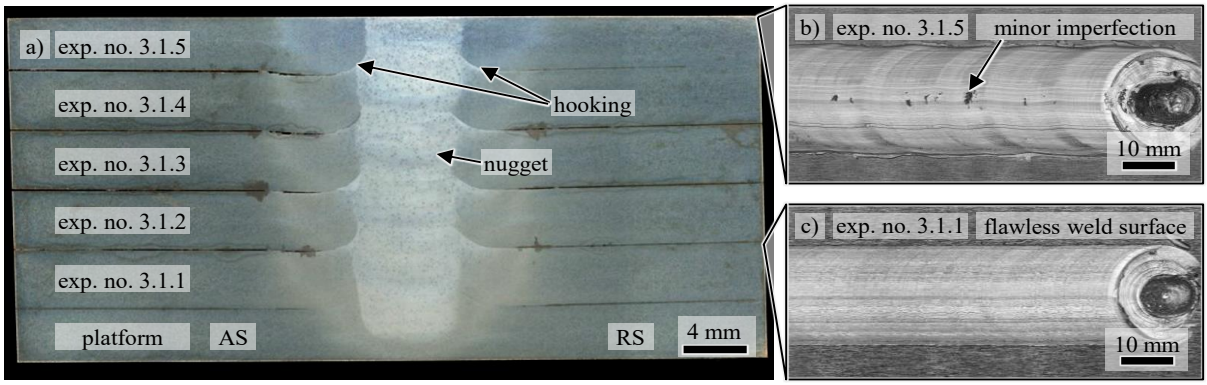

Fig. 8: a) Etched cross section of the additive build (exp. no. 3.1) with photographs of the weld surfaces from the fifth (*class* c, exp. no. 3.1.5) und the first layer (*class a*, exp. no. 3.1.1)

Conclusions and Outlook

Three studies were conducted to improve the weld surfaces, thereby enabling a direct build-up without surface machining and a material utilization ratio regarding the build heights $p_{mur,\,h}$ of 100%. In studies 1 and 2, different FSW tools were investigated in terms of their effect on the weld surface quality, the weld morphology (i.e., internal defects), and the shear strength. Based on that, three five-layer (excluding the platform) additive builds were produced without surface machining. The most important conclusions are:

- The surface and the internal quality of friction stir lap welds can be improved using an FSW tool with both a rotating and a stationary shoulder.
- The maximum shear strength of friction stir lap welds is influenced by hooking. Cavities did not reduce the overall weld strength.
- It is possible to produce at least four flawless layers using FSAM without surface machining.
- It is hypothesized that defects in the higher layers of the FSAM builds were caused by an insufficient decompression due to an increased gap between the aluminum sheets. The data suggests that the effect of these gaps on the weld surface quality and the formation of cavities can be compensated by welding with higher temperatures T_p and axial forces F_z.

- For an improved efficiency of the process for flawless builds consisting of more than four layers it is suggested to only machine every fourth layer. Further investigations need to be carried out regarding this process strategy.

Acknowledgements

The authors would like to thank Annette Lietz for preparing the cross sections for the metallographic analysis.

Author Contributions

Conceptualization, M.E.S.; methodology M.E.S.; software, M.E.S. and P.D.; validation, M.E.S and P.D.; formal analysis, M.E.S.; investigation, M.E.S. and P.D.; resources, M.E.S.; data curation, M.E.S. and P.D.; writing – original draft preparation, M.E.S.; writing – review and editing, R.H., C.B and M.F.Z.; visualization, M.E.S. and P.D.; supervision, M.F.Z.; project administration, M.E.S.; funding acquisition M.F.Z. All authors have read and agreed to the published version of the manuscript.

Conflicts of Interest

The authors declare that they have no conflict of interest.

Appendix

Table 3: Process parameters and welding results of studies 1 and 2; non-existent data is marked with "–". The best welding results are highlighted in green. The process parameter sets used for study 3 (Table 4) are highlighted in grey.

Exp. no.	Process parameters			Welding results										
					Seam underfill			Flash height				Shear force		
	Temp. T_p	Welding speed v	Axial force F_z	Surf. qual. class	Mean $\bar{h}_{su}$	Max. $\hat{h}_{su}$	Sd. $h_{su,\,sd}$	Mean $\bar{h}_f$	Max. $\hat{h}_f$	Sd. $h_{f,\,sd}$	Cavities	Mean $\bar{F}_n$	Max. $\hat{F}_n$	Sd. $F_{n,\,sd}$
	in °C	in mm/min	in kN	–	in mm			in mm			y/n	in kN		
1.1	480	100	6.5	*d*	–	–	–	–	–	–	y	–	–	–
1.2	480	200	6.5	*d*	–	–	–	–	–	–	y	–	–	–
1.3	480	100	7.5	*b*	0.41	0.96	0.15	0.85	4.32	0.94	y	8.97	9.14	0.15
1.4	480	200	7.5	*d*	–	–	–	–	–	–	y	–	–	–
1.5	500	100	6.5	*d*	–	–	–	–	–	–	y	–	–	–
1.6	500	200	6.5	*c*	–	–	–	–	–	–	y	9.18	9.44	0.19
1.7	500	100	7.5	*b*	0.53	1.18	0.25	3.06	5.95	1.85	n	7.42	7.77	0.27
1.8	500	200	7.5	*c*	–	–	–	–	–	–	y	9.60	9.65	0.05
1.9	490	150	7.0	*c*	–	–	–	–	–	–	y	9.54	9.63	0.12
1.10	490	50	7.0	*b* [1]	–	–	–	–	–	–	–	–	–	–
1.11	490	250	7.0	*d*	–	–	–	–	–	–	y	–	–	–
1.12	490	150	6.0	*d*	–	–	–	–	–	–	y	–	–	–
1.13	490	150	8.0	*b*	0.31	0.85	0.17	2.27	6.03	1.51	y	9.60	9.97	0.36
1.14	470	150	7.0	*d*	–	–	–	–	–	–	y	–	–	–
1.15	510	150	7.0	*c*	–	–	–	–	–	–	y	7.80	7.86	0.08
2.1	480	50	7.5	*a*	0.12	0.43	0.09	0.11	0.53	0.09	y	6.79	7.31	0.37
2.2	480	80	7.5	*c*	–	–	–	–	–	–	y	10.70	11.11	0.51
2.3	480	50	8.5	*a*	0.12	0.45	0.10	0.15	0.76	0.16	n	7.36	7.61	0.34
2.4	480	80	8.5	*a*	0.13	0.47	0.09	0.07	0.67	0.12	y	10.33	10.96	0.45
2.5	500	50	7.5	*a*	0.13	0.55	0.12	0.16	0.66	0.14	y	6.68	6.77	0.08
2.6	500	80	7.5	*a*	0.08	0.36	0.09	0.16	0.82	0.17	n	8.33	8.85	0.41
2.7	500	50	8.5	*a*	0.15	0.48	0.10	0.20	0.94	0.13	y	6.31	6.46	0.11
2.8	500	80	8.5	*a*	0.08	0.49	0.12	0.17	0.68	0.15	n	6.44	6.54	0.12
2.9	490	65	8.0	*a*	0.12	0.46	0.10	0.16	1.05	0.16	n	6.64	7.08	0.31
2.10	490	35	8.0	*a*	0.16	0.52	0.11	0.22	0.88	0.11	n	7.19	7.31	0.13
2.11	490	95	8.0	*a*	0.07	0.45	0.10	0.07	0.46	0.11	y	10.09	10.71	0.46
2.12	490	65	7.0	*a*	0.09	0.46	0.10	0.14	0.67	0.16	y	7.58	7.94	0.48
2.13	490	65	9.0	*a*	0.11	0.45	0.10	0.16	0.60	0.10	y	7.75	7.98	0.20
2.14	470	65	8.0	*a*	0.07	0.50	0.11	0.08	0.87	0.13	y	9.54	9.67	0.12
2.15	510	65	8.0	*a*	0.13	0.50	0.13	0.19	0.60	0.17	y	9.55	9.80	0.18

[1]Exp. no. 1.10 had to be stopped prematurely due to process instabilities and was therefore not analyzed any further.

Temp.: temperature, max.: maximum, sd.: standard deviation, suf. qual.: surface quality, y: yes, n: no

Table 4: Process parameters and welding results of study 3; the best welding results are highlighted in green.

Exp. no.	Process parameters			Welding results								
	Temp. T_p	Welding speed v	Axial force F_z	Surf. qual. class	Seam underfill			Flash height			Cavities
					Mean $\bar{h}_{su}$	Max. $\hat{h}_{su}$	Sd. $h_{su,\,sd}$	Mean $\bar{h}_f$	Max. $\hat{h}_f$	Sd. $h_{f,\,sd}$	
	in °C	in mm/min	in kN	–	in mm			in mm			y/n
3.1.1	500	80	8.5	*a*	0.04	0.47	0.10	0.16	0.57	0.12	n
.2				*a*	0.08	0.74	0.09	0.17	0.47	0.08	n
.3				*a*	0.16	0.59	0.10	0.13	0.55	0.12	n
.4				*a*	0.21	0.51	0.10	0.17	0.52	0.11	n
.5				*c*	0.22	0.61	0.12	0.16	0.60	0.09	n
3.2.1	490	65	8.0	*a*	0.06	0.50	0.11	0.17	0.53	0.11	n
.2				*a*	0.12	0.93	0.11	0.15	0.48	0.08	n
.3				*a*	0.17	0.73	0.10	0.19	0.37	0.09	n
.4				*c*	0.24	0.96	0.12	0.14	1.06	0.10	n
.5				*d*	0.27	0.97	0.12	0.18	1.28	0.12	y
3.3.1	490	95	8.0	*a*	0.03	0.51	0.11	0.12	1.15	0.18	n
.2				*a*	0.07	0.72	0.10	0.10	0.51	0.12	n
.3				*a*	0.13	0.71	0.09	0.10	0.59	0.13	n
.4				*c*	0.19	0.93	0.11	0.07	0.79	0.12	y
.5				*d*	0.39	1.83	0.35	0.14	1.45	0.21	y

Temp.: temperature, max.: maximum, sd.: standard deviation, suf. qual.: surface quality, y: yes, n: no

References

[1] S. Palanivel, H. Sidhar, R.S. Mishra, Friction Stir Additive Manufacturing: Route to High Structural Performance, JOM 67 (2015) 3, pp. 616–621.

[2] S. Palanivel, P. Nelaturu, B. Glass, R.S. Mishra, Friction stir additive manufacturing for high structural performance through microstructural control in an Mg based WE43 alloy, Materials & Design 65 (2015), pp. 934–952.

[3] M. Yuqing, K. Liming, H. Chunping, L. Fencheng, L. Qiang, Formation characteristic, microstructure, and mechanical performances of aluminum-based components by friction stir additive manufacturing, International Journal of Advanced Manufacturing Technology 83 (2016) 9–12, pp. 1637–1647.

[4] M. Ruhstorfer, Rührreibschweißen von Rohren (Translated title: „Friction stir welding of pipes“), utzverlag, Munich, Germany, 2012. ISBN: 978-3-8316-4197-0.

[5] R. Hartl, A. Bachmann, S. Liebl, A. Zens, M.F. Zaeh, Automated surface inspection of friction stir welds by means of structured light projection, IOP Conference Series: Materials Science and Engineering 480 (2019), 012035.

[6] G. Buffa, L. Fratini, F. Impero, A. Masnata, F. Scherillo, A. Squillace, Surface and mechanical characterization of stationary shoulder friction stir welded lap joints: experimental and numerical approach, International Journal of Material Forming 13 (2020) 5, pp. 725–736.

[7] Z. Zhao, X. Yang, S. Li, D. Li, Interfacial bonding features of friction stir additive manufactured build for 2195-T8 aluminum-lithium alloy, Journal of Manufacturing Processes 38 (2019), pp. 396–410.

[8] Z. Zhang, Z.J. Tan, J.Y. Li, Y.F. Zu, W.W. Liu, J.J. Sha, Experimental and numerical studies of re-stirring and re-heating effects on mechanical properties in friction stir additive manufacturing, International Journal of Advanced Manufacturing Technology 104 (2019) 1–4, pp. 767–784.

[9] G. Costanzi, A. Bachmann, M.F. Zäh, Entwicklung eines FSW-Spezialwerkzeugs zur Messung der Schweißtemperatur (Translated title: „Development of a special FSW tool for measuring the welding temperature“), in: Research Association on Welding and Allied Processes of the DVS, DVS Media, Duesseldorf, Germany, 2017, pp. 119 – 125. ISBN: 978-3-96144-008-5.

[10] A. Bachmann, M. Krutzlinger, M.F. Zaeh, Influence of the welding temperature and the welding speed on the mechanical properties of friction stir welds in EN AW-2219-T87, IOP Conference Series: Materials Science and Engineering 373 (2018), 012016.

[11] A. Bachmann, J. Gamper, M. Krutzlinger, A. Zens, M.F. Zaeh, Adaptive model-based temperature control in friction stir welding, The International Journal of Advanced Manufacturing Technology 93 (2017) 1–4, pp. 1157–1171.
[12] M.E. Sigl, A. Bachmann, T. Mair, M.F. Zaeh, Torque-Based Temperature Control in Friction Stir Welding by Using a Digital Twin, Metals 10 (2020) 7, 914.
[13] M. Momeni, M. Guillot, Effect of Tool Design and Process Parameters on Lap Joints Made by Right Angle Friction Stir Welding (RAFSW), Journal of Manufacturing and Materials Processing 3 (2019) 3, 66.
[14] C.B. Fuller, Friction Stir Tooling: Tool Materials and Designs, in: Friction stir welding and processing, ASM International, Materials Park, Ohio, USA, 2007, pp. 7–35. ISBN: 978-0-87170-840-3.
[15] H. Shirazi, S. Kheirandish, M.A. Safarkhanian, Effect of process parameters on the macrostructure and defect formation in friction stir lap welding of AA5456 aluminum alloy, Measurement 76 (2015), pp. 62–69.
[16] E. Aldanondo, J. Vivas, P. Álvarez, I. Hurtado, Effect of Tool Geometry and Welding Parameters on Friction Stir Welded Lap Joint Formation with AA2099-T83 and AA2060-T8E30 Aluminium Alloys, Metals 10 (2020) 7, 872.